
Article:
Savoury, C.D.J., Littlefair, S.P. orcid.org/0000-0001-7221-855X, Dhillon, V.S. et al. (6 more authors) (2011) Cataclysmic variables below the period gap: mass determinations of 14 eclipsing systems. Monthly Notices of the Royal Astronomical Society , 415. pp. 2025-2041. ISSN 0035-8711

https://doi.org/10.1111/j.1365-2966.2011.18707.x

Table 3. System parameters derived using the probability density functions shown in Fig. 4. R_r is the volume radius of the secondary's Roche lobe (Eggleton 1983). The errors quoted are statistical errors of the fitting process and do not include systematic effects such as those discussed in section 3.3.

	CTCV J1300-3052	**CTCV J2354-4700**	**SDSS J1152+4049**	**OU Vir**	**DV UMa**	**XZ Eri**	**SDSS 1702**
q	0.240 ± 0.021	0.1097 ± 0.0008	0.155 ± 0.006	0.1641 ± 0.0013	0.1778 ± 0.0022	0.118 ± 0.003	0.248 ± 0.005
$M_w/M_\odot$	0.736 ± 0.014	0.935 ± 0.031	0.560 ± 0.028	0.703 ± 0.012	1.098 ± 0.024	0.769 ± 0.017	0.91 ± 0.03
$R_w/R_\odot$	0.01111 ± 0.00018	0.0089 ± 0.0003	0.0135 ± 0.0004	0.01191 ± 0.00017	0.00703 ± 0.00028	0.01081 ± 0.00022	0.0092 ± 0.0004
$\log g$	8.21 ± 0.02	8.51 ± 0.04	7.93 ± 0.05	8.13 ± 0.02	8.78 ± 0.04	8.26 ± 0.03	8.47 ± 0.05
$T_w(K)$	11100 ± 800	14800 ± 700	12400 ± 1400	22300 ± 2100	15500 ± 2400	15300 ± 1900	15200 ± 1200
$M_r/M_\odot$	0.177 ± 0.021	0.101 ± 0.003	0.087 ± 0.006	0.1157 ± 0.0022	0.196 ± 0.005	0.091 ± 0.004	0.223 ± 0.010
$R_r/R_\odot$	0.215 ± 0.008	0.1463 ± 0.0016	0.142 ± 0.003	0.1634 ± 0.0010	0.2176 ± 0.0018	0.1350 ± 0.0018	0.252 ± 0.004
$a/R_\odot$	0.813 ± 0.011	0.692 ± 0.008	0.606 ± 0.010	0.686 ± 0.004	0.892 ± 0.006	0.621 ± 0.005	0.945 ± 0.012
K_w (kms^{-1})	90 ± 8	51.9 ± 0.6	60 ± 3	66.4 ± 0.6	78.9 ± 1.0	53.6 ± 1.5	94.0 ± 2.2
K_r (kms^{-1})	372.2 ± 2.5	482 ± 6	387 ± 6	403.0 ± 2.3	443 ± 3	452 ± 3	380 ± 4
i°	86.3 ± 1.1	89.26 ± 0.28	82.38 ± 0.23	79.60 ± 0.04	82.93 ± 0.10	80.02 ± 0.12	82.55 ± 0.17
d (pc)	375 ± 13	674 ± 19	543 ± 21	570 ± 70	504 ± 30	371 ± 19	270 ± 16
P_{orb} (mins)	128.0746325(14)*	94.3923889(14)*	97.518753(4)*	104.696803(7)[1]	123.6278190(20)[2]	88.069667(7)[2]	144.11821(13)[3]
	SDSS 1035	**SDSS 1507**	**SDSS 0903**	**SDSS 1227**	**SDSS 1433**	**SDSS 1502**	**SDSS 1501**
q	0.0571 ± 0.0010	0.0647 ± 0.0018	0.113 ± 0.004	0.1115 ± 0.0016	0.0661 ± 0.0007	0.1099 ± 0.0007	0.101 ± 0.010
$M_w/M_\odot$	0.835 ± 0.009	0.892 ± 0.008	0.872 ± 0.011	0.796 ± 0.018	0.865 ± 0.005	0.709 ± 0.004	0.767 ± 0.027
$R_w/R_\odot$	0.00991 ± 0.00010	0.00956 ± 0.00013	0.00947 ± 0.00019	0.01052 ± 0.00022	0.00962 ± 0.00006	0.01145 ± 0.00005	0.0107 ± 0.0003
$\log g$	8.37 ± 0.01	8.45 ± 0.01	8.42 ± 0.02	8.29 ± 0.02	8.41 ± 0.01	8.17 ± 0.01	8.26 ± 0.04
$T_w(K)$	10000 ± 1100	11300 ± 1000	13300 ± 1700	15900 ± 1400	12700 ± 1500	11800 ± 1200	10800 ± 1500
$M_r/M_\odot$	0.0475 ± 0.0012	0.0575 ± 0.0020	0.099 ± 0.004	0.0889 ± 0.0025	0.0571 ± 0.0007	0.0781 ± 0.0008	0.077 ± 0.010
$R_r/R_\odot$	0.1047 ± 0.0008	0.0969 ± 0.0011	0.1358 ± 0.0020	0.1365 ± 0.0013	0.1074 ± 0.0004	0.1241 ± 0.0003	0.122 ± 0.005
$a/R_\odot$	0.5977 ± 0.0022	0.5329 ± 0.0019	0.632 ± 0.003	0.640 ± 0.005	0.5869 ± 0.0012	0.5844 ± 0.0013	0.588 ± 0.008
K_w (kms^{-1})	28.5 ± 0.6	35.1 ± 1.0	54.6 ± 2.0	51.3 ± 0.8	33.8 ± 0.3	50.4 ± 0.4	48 ± 5
K_r (kms^{-1})	499.3 ± 1.5	543.7 ± 1.2	481.7 ± 1.9	460 ± 3	511.1 ± 0.9	456.5 ± 0.8	470.5 ± 3.2
i°	83.98 ± 0.08	83.47 ± 0.12	82.09 ± 0.19	84.29 ± 0.10	84.36 ± 0.05	88.35 ± 0.17	82.8 ± 0.5
d (pc)	174 ± 12	168 ± 12	299 ± 14	400 ± 13	226 ± 12	175 ± 11	306 ± 21
P_{orb} (mins)	82.08965(29)[4,6]	66.61192(6)[5,6]	85.065902(13)[6]	90.661019(10)[6]	78.106657(3)[6]	84.82984(7)[6]	81.85141771(28)*

*This paper; [1]Feline et al. 2004a; [2]Feline et al. 2004b; [3]Littlefair et al. 2006a; [4]Littlefair et al. 2006b; [5]Littlefair et al. 2007; [6]Littlefair et al. 2008;

Mon. Not. R. Astron. Soc. **000**, 1–18 (2010) Printed 15 March 2011 (MN LATEX style file v2.2)

Cataclysmic Variables below the Period Gap: Mass Determinations of 14 Eclipsing Systems

C. D. J. Savoury[1⋆], S. P. Littlefair[1], V. S. Dhillon[1], T. R. Marsh[2], B. T. Gänsicke[2], C. M. Copperwheat[2], P. Kerry[1], R. D. G. Hickman[2] and S. G. Parsons[2]
[1] *Dept of Physics and Astronomy, University of Sheffield, Sheffield, S3 7RH, UK*
[2] *Dept of Physics, University of Warwick, Coventry, CV4 7AL, UK*

Submitted for publication in the Monthly Notices of the Royal Astronomical Society 15 March 2011

ABSTRACT

We present high-speed, three-colour photometry of the eclipsing cataclysmic variables CTCV J1300-3052, CTCV J2354-4700 and SDSS J115207.00+404947.8. These systems have orbital periods of 128.07, 94.39 and 97.52 minutes respectively, placing all three systems below the observed "period gap" for cataclysmic variables. For each system we determine the system parameters by fitting a parameterised model to the observed eclipse light curve by χ^2 minimisation.

We also present an updated analysis of all other eclipsing systems previously analysed by our group. The updated analysis utilises Markov Chain Monte Carlo techniques which enable us to arrive confidently at the best fits for each system with more robust determinations of our errors. A new bright spot model is also adopted, that allows better modelling of bright-spot dominated systems. In addition, we correct a bug in the old code which resulted in the white dwarf radius being underestimated, and consequently both the white dwarf and donor mass being overestimated. New donor masses are generally between 1 and 2σ of those originally published, with the exception of SDSS 1502 (-2.9σ, $\Delta M_r = -0.012 M_\odot$) and DV UMa ($+6.1\sigma$, $\Delta M_r = +0.039 M_\odot$). We note that the donor mass of SDSS 1501 has been revised upwards by $0.024 M_\odot$ ($+1.9\sigma$). This system was previously identified as having evolved passed the minimum orbital period for cataclysmic variables, but the new mass determination suggests otherwise. Our new analysis confirms that SDSS 1035 and SDSS 1433 have evolved past the period minimum for cataclysmic variables, corroborating our earlier studies.

We find that the radii of donor stars are oversized when compared to theoretical models, by approximately 10 percent. We show that this can be explained by invoking either enhanced angular momentum loss, or by taking into account the effects of star spots. We are unable to favour one cause over the other, as we lack enough precise mass determinations for systems with orbital periods between 100 and 130 minutes, where evolutionary tracks begin to diverge significantly.

We also find a strong tendency towards high white dwarf masses within our sample, and no evidence for any He-core white dwarfs. The dominance of high mass white dwarfs implies that erosion of the white dwarf during the nova outburst must be negligible, or that not all of the mass accreted is ejected during nova cycles, resulting in the white dwarf growing in mass.

Key words: binaries: close - binaries: eclipsing - stars: dwarf novae - stars: low mass, brown dwarfs - stars: novae, cataclysmic variables - stars: evolution.

1 INTRODUCTION

Cataclysmic variable stars (CVs) are a class of interacting binary system undergoing mass transfer from a Roche-lobe filling secondary to a white dwarf primary, usually via a gas stream and accretion disc. A bright spot is formed where

⋆ E-mail:chris.savoury@sheffield.ac.uk

the gas stream collides with the edge of the accretion disc, often resulting in an 'orbital hump' in the light curve at phases $0.6 - 1.0$ due to the area of enhanced emission rotating into our line of sight. For an excellent overview of CVs, see Warner (1995) and Hellier (2001). The light curves of eclipsing CVs can be quite complex, with the accretion disc, white dwarf and bright spot all being eclipsed in rapid succession. When observed with time resolutions of the order of a few seconds, this eclipse structure allows the system parameters to be determined to a high degree of precision with relatively few assumptions (Wood et al. 1986). Over the last eight years our group has used the high-speed, three-colour camera ULTRACAM (Dhillon et al. 2007) to obtain such time-resolution. The ability to image in three different wave-bands simultaneously makes ULTRACAM an ideal tool to study the complex, highly variable light curves of CVs. Using ULTRACAM data, we have obtained system parameters for several short period systems (e.g. Feline et al. 2004a, 2004b; Littlefair et al. 2006a, 2007, 2008), including the first system accreting from a sub-stellar donor (Littlefair et al. 2006b).

Despite extensive study over recent decades, there are still several outstanding issues with evolutionary theories of CVs that have wide ranging implications for all close binary systems. The secular evolution of CVs is driven by angular momentum losses from the binary orbit. In the standard model, systems with orbital periods below ∼130 minutes are thought to lose angular momentum via gravitational radiation. Angular momentum losses sustain mass transfer and subsequently drive the system to shorter orbital periods, until the point where the donor star becomes degenerate (e.g. Paczynski 1981). Here, the donor star is driven out of thermal equilibrium and begins to expand in response to mass-loss, driving the system to longer orbital periods. We therefore expect to observe a period cut-off around $P_{orb} \simeq 65-70$ minutes, dubbed the "period minimum", in addition to a build up of systems at this minimum period (the "period spike"; Kolb & Baraffe 1999). The period spike has recently been identified by Gänsicke et al. (2009), whose study of SDSS CVs found an accumulation of systems with orbital periods between 80 and 86 minutes. This is significantly longer than expected. A larger than expected orbital period implies that the orbital separation is larger than expected, nd thus the radii of the donor star must also be larger than expected in order to remain Roche-lobe filling. Recent observations by Littlefair et al. (2008) support this, suggesting that the donor stars in short period CVs are roughly 10 percent larger than predicted by the models of Kolb & Baraffe (1999). The reason why the donor stars appear oversized remains uncertain. Possible explanations include some form of enhanced angular momentum loss (e.g. Patterson 1998; Kolb & Baraffe 1999; Willems et al. 2005) which would increase mass loss and drive the donor stars further from thermal equilibrium, or missing stellar physics in the form of magnetic activity coupled with the effects of rapid rotation (e.g. Chabrier et al. 2007).

One way to determine why the donor stars appear oversized is to compare the shape of the observed donor mass-period relationship ($M_2 - P_{orb}$), and by implication, mass-radius ($M_2 - R_2$) relationship, to the models of Kolb & Baraffe (1999), calculated with enhanced angular momentum loss or modified stellar physics. These models, in principle, make different predictions for the shape of the mass-period relationship and the position of the period minimum. Both the shape of the mass-period relationship and the position of the period minimum are dependent on the ratio $\kappa = \tau_M/\tau_{KH}$, where τ_M and τ_{KH} are the mass-loss and thermal timescales of the donor star respectively. Initially, $\kappa \gg 1$, and the donor is able to contract in response to mass-loss. As the system evolves to shorter orbital periods both timescales increase, although the thermal timescale increases much faster than the mass-loss timescale. This results in κ decreasing with orbital period. When the two timescales become comparable, the donor is unable to contract rapidly enough to maintain thermal equilibrium and becomes oversized for a given mass. Since donor expansion does not occur until the thermal and mass-loss timescales become comparable, if enhanced angular momentum loss is responsible for the oversized CV donors, the systems *immediately* below the period gap would not be expected to be far from thermal equilibrium. In contrast, star spots would inhibit the convective processes in all CV donors below the period gap (assuming of course that spot properties are similar at all masses). Models that include the effects of enhanced angular momentum loss and star spot coverage therefore begin to diverge significantly in $\dot{M}$ and M_2 at orbital periods of 100 minutes. We can distinguish between these models if we have a sample of CVs that covers a wide range of orbital periods and whose component masses and radii are known to a high degree of precision (e.g. $\sigma M_2 \sim 0.005 M_\odot$). Unfortunately we lack enough precise mass-radii determinations for systems with orbital periods between 95 and 130 minutes. To overcome this shortage we observed eclipses of three CVs below the period gap: CTCV J1300-3052, CTCV J2354-4700 and SDSS J115207.00+404947.8 (hereafter CTCV 1300, CTCV 2354 and SDSS 1152).

CTCV 2354 and CTCV 1300 were discovered as part of the Calán-Tololo Survey follow up (Tappert et al. 2004). During the follow up, both systems were found to be eclipsing with orbital periods of 94.4 and 128.1 minutes, respectively. Basic, non-time resolved, spectroscopic data was obtained for each system. The spectrum of CTCV 1300 showed features typical of the three main components in CVs: strong emission lines from the accretion disc, broad, shallow absorption features from the white dwarf and red continuum and absorption bands from the donor. CTCV 2354 was found to contain strong emission lines of H and He, generally typical of a dwarf nova in quiescence.

SDSS 1152 was identified as a CV by Szkody et al. (2007). The system shows broad, double-peaked, Balmer emission lines, which are characteristic of a high-inclination accreting binary. Follow up work by Southworth et al. (2010) found the system to have an orbital period of 97.5 minutes.

In this paper we present ULTRACAM light curves of CTCV 1300 ($u'g'r'i'$), CTCV 2354 ($u'g'r'$) and SDSS 1152 ($u'g'r'$), and in each case attempt to determine the system parameters via light curve modelling. In addition, we also present an updated analysis of all eclipsing systems previously published by our group: OU Vir (Feline et al. 2004a), XZ Eri and DV UMa (Feline et al. 2004b), SDSS J1702+3229 (Littlefair et al. 2006a), SDSS J1035+0551 (Littlefair et al. 2006b, 2008), SDSS J150722+523039 (Littlefair et al. 2007, 2008), SDSS J0903+3300, SDSS

J1227+5139, SDSS J1433+1011, SDSS J1501+5501 and SDSS J1502+3334 (Littlefair et al. 2008). Our primary reason for doing so was the introduction of a new analysis utilising Markov Chain Monte Carlo (MCMC) techniques and an updated bright spot model. The MCMC analysis is more reliable at converging to a best fit than the downhill simplex algorithm used previously, while the new bright spot model allows for a more realistic modelling of bright spot dominated systems (e.g. CTCV 1300, DV UMa, SDSS 1702) and should thus provide more accurate values of the mass ratio, q. While implementing these changes, we also discovered a bug in the code previously used to bin the light curves (see e.g. Littlefair et al. 2006a for details of the original code) which resulted in the white dwarf radius being underestimated, and consequently, the white dwarf and donor mass being overestimated. Full details are provided in section 3.3.

2 OBSERVATIONS

In Table 1 we present details of the observations used to analyse CTCV 1300, CTCV 2354, SDSS 1152 and SDSS 1501. For observations of other systems we refer the reader to table 1 in the following publications: Feline et al. 2004a (OU Vir), Feline et al. 2004b (XZ Eri and DV UMa), Littlefair et al. 2006a (SDSS 1702), Littlefair et al. 2007 (SDSS 1507) and Littlefair et al. 2008 (SDSS 0903, SDSS 1227, SDSS 1433, SDSS 1501 and SDSS 1502).

For reasons outlined in section 3.3 we do not use the SDSS 1501 data listed in Littlefair et al. (2008). Instead we model a single eclipse observed in 2004 (Table 1). Not all of the eclipses listed in Table 1 are used for determining system parameters. This is because the eclipses have poor signal-to-noise, or lack clear bright spot features. The eclipses not used for determining system parameters are however still used to refine our orbital ephemerides (section 3.1). These eclipses include CTCV 2354 cycle numbers 11197, 11198, 11366, 11396, 11457, 11472 and SDSS 1501 cycles 24718 and 24719. CTCV 2354 cycle numbers 16156, 16676 and CTCV 1300 cycle number 12888 are analysed separately in section 3.4 because the shape of the eclipse has changed significantly in comparison to the 2007 data (see section 3.2).

Data reduction was carried out in a standard manner using the ULTRACAM pipeline reduction software, as described in Feline (2005) and Dhillon et al. (2007). A nearby comparison star was used to correct the data for transparency variations. Observations of the standard stars G162-66, G27-45 and G93-48 were used to correct the magnitudes to the standard SDSS system (Smith et al. 2002). Due to time constraints and poor weather, we were unable to observe a standard star to flux calibrate our data for SDSS 1152. Consequently, we have used the Sloan magnitudes of the comparison stars and corrected for different instrumental response. To do this, we use measured response curves for filters and dichroics to create overall response curves for ULTRACAM. These are then combined with curves of theoretical extinction and library spectra (Pickles 1998) to obtain synthetic ULTRACAM colours. The same process is then repeated for the SDSS colour set, with the difference between the two sets being the correction applied.

Table 2. Orbital ephemerides.

Object	T_0 (HJD)	$P_{\rm orb}$ (d)
CTCV 1300	2454262.599146 (8)	0.088940717 (1)
CTCV 2354	2454261.883885 (5)	0.065550270 (1)
SDSS 1152	2455204.601298 (6)	0.067721356 (3)
SDSS 1501	2453799.710832 (3)	0.0568412623(2)

3 RESULTS

3.1 Orbital ephemerides

The times of white dwarf mid-ingress T_{wi} and mid-egress T_{we} were determined by locating the minimum and maximum times, respectively, of the smoothed light-curve derivative. Mid-eclipse times, T_{mid}, were determined by assuming the white dwarf eclipse to be symmetric around phase one and taking $T_{mid} = (T_{wi} + T_{we})/2$. Eclipse times were taken from the literature for CTCV 1300, CTCV 2354 (Tappert et al. 2004), SDSS 1501 (Littlefair et al. 2008) and SDSS 1152 (Southworth et al. 2010) and combined with our mid-eclipse times shown in Table 1. The errors on our data were adjusted to give $\chi^2 = 1$ with respect to a linear fit. In each case we observe no cycle ambiguity. We do however, observe a significant, O-C offset between our data and the times published by Tappert et al. (2004) for CTCV 1300 and CTCV 2354. For CTCV 1300, the average difference is 165.9 seconds, while for CTCV 2354 it is 148.0 seconds. We believe this to be due to the differing methods of calculating T_{mid}; Tappert et al. (2004) calculated T_{mid} by fitting a parabola to the overall eclipse structure, whereas we determined T_{mid} from the white dwarf eclipse. We therefore subtract these average offsets from the published literature values and take the resulting O-C difference as our uncertainty on that time. Where possible, we averaged the measured mid-eclipse times in the r' and g' bands to fit the ephemeris. Due to the low signal-to-noise of the eclipse of CTCV 2354 in May 2010, measuring the times of white dwarf mid-ingress T_{wi} and mid-egress T_{we} was not possible. Consequently, the eclipse times and errors were measured by eye in the g' and r' bands and then averaged in order to estimate the cycle number. This time was not used to refine the ephemeris but is included for completeness. The ephemerides found are shown in Table 2.

3.2 Light curve morphology and variations

3.2.1 CTCV J1300-3052

Fig. 1 (top) shows the two observed eclipses of CTCV 1300 from the 2007 data set folded on orbital phase in the g' band. The white dwarf ingress and egress features are clearly visible at phases 0.965 and 1.040, respectively, as are the bright spot features at phases 0.960 and 1.085. These features dominate the light curve, which follows a typical dwarf nova eclipse shape (e.g. Littlefair et al. 2006a, 2007, 2008). The depth of the bright spot eclipse indicates that the bright spot is the dominant source of light in this system, while the eclipse of the accretion disc is difficult to discern by eye, indicating that the accretion disc contributes little light to this system. Closer inspection of the eclipses from each night reveals a noticeable difference in the shape of the bright spot ingress feature. This is caused by heavy pre-eclipse flickering,

Table 1. Journal of observations. The dead-time between exposures was 0.025 s for all observations. The relative GPS time stamping on each data point is accurate to 50 μs. Instr setup denotes the telescope (WHT, NTT or VLT) and instrument used for each observation, where UCAM and USPEC represent ULTRACAM and ULTRASPEC, respectively. Phase Cov corresponds to the phase coverage of the eclipse, taking the eclipse of the white dwarf as phase 1. T_{exp} and N_{exp} denote the exposure time, and number of exposures, respectively.

Date	Object	Instr setup	T_{mid} (HMDJ)	Cycle	Phase Cov	Filters	T_{exp} (s)	N_{exp}	Seeing (")
2007 June 09	CTCV 2354	VLT+UCAM	54261.383926(25)	0	0.73–1.08	$u'g'r'$	2.22	821	0.6–1.0
2007 June 13	CTCV 2354	VLT+UCAM	54265.316786(61)	60	0.70–1.11	$u'g'r'$	4.92	473	0.8–1.2
2007 June 15	CTCV 2354	VLT+UCAM	54267.348921(21)	91	0.78–1.08	$u'g'r'$	2.22	779	0.6–0.7
2007 June 15	CTCV 2354	VLT+UCAM	54267.414476(20)	92	0.74–1.05	$u'g'r'$	2.22	757	0.6–0.7
2007 June 16	CTCV 2354	VLT+UCAM	54268.397717(20)	107	0.72–1.06	$u'g'r'$	2.22	845	0.6–1.1
2007 June 19	CTCV 2354	VLT+UCAM	54271.413077(21)	153	0.82–1.15	$u'g'r'$	2.22	826	0.6–1.0
2007 June 20	CTCV 2354	VLT+UCAM	54272.396368(29)	168	0.50–1.50	$u'g'r'$	2.32	2390	0.6–1.0
2007 June 21	CTCV 2354	VLT+UCAM	54273.314054(5)	182	0.86–1.20	$u'g'r'$	1.96	931	1.2–2.4
2007 June 21	CTCV 2354	VLT+UCAM	54273.379579(3)	183	0.77–1.09	$u'g'r'$	1.96	916	0.9–1.5
2009 June 12	CTCV 2354	NTT+USPEC	54995.350263(6)	11197	0.65–1.35	g'	9.87	482	1.4–2.6
2009 June 12	CTCV 2354	NTT+USPEC	54995.415961(6)	11198	0.35–1.17	g'	9.87	482	1.0–2.2
2009 June 23	CTCV 2354	NTT+USPEC	55006.428224(2)	11366	0.66–1.16	g'	3.36	817	1.4–2.2
2009 June 25	CTCV 2354	NTT+USPEC	55008.394766(1)	11396	0.70–1.22	g'	3.36	855	1.2–2.0
2009 June 29	CTCV 2354	NTT+USPEC	55012.393334(1)	11457	0.55–1.37	g'	2.98	1593	0.8–2.4
2009 June 30	CTCV 2354	NTT+USPEC	55013.376588(1)	11472	0.30–1.55	g'	1.96	3592	1.2–2.0
2010 May 03	CTCV 2354	NTT+UCAM	55320.414(2)	16156	0.43–1.21	$u'g'r'$	8.23	526	1.4–1.8
2010 June 06	CTCV 2354	NTT+UCAM	55354.434846(24)	16676	0.47–1.19	$u'g'r'$	3.84	1048	1.0–1.2
2007 June 10	CTCV 1300	VLT+UCAM	54262.099145(3)	0	0.72–1.20	$u'g'r'$	1.00	3462	0.6–1.2
2007 June 13	CTCV 1300	VLT+UCAM	54262.123093(8)	34	0.74–1.15	$u'g'i'$	1.95	1573	0.6–1.1
2010 June 07	CTCV 1300	NTT+UCAM	55355.002677(1)	12288	0.85–1.12	$u'g'r'$	2.70	511	0.8–1.1
2010 Jan 07	SDSS 1152	WHT+UCAM	55204.101282(9)	0	0.16–1.13	$u'g'r'$	3.80	1492	2.0–3.8
2010 Jan 07	SDSS 1152	WHT+UCAM	55204.169031(8)	1	0.72–1.12	$u'g'r'$	3.80	600	1.4–2.5
2010 Jan 07	SDSS 1152	WHT+UCAM	55204.236742(7)	2	0.85–1.12	$u'g'r'$	3.80	415	1.2–3.2
2004 May 17	SDSS 1501	WHT+UCAM	53142.921635(6)	-11546	0.80–1.21	$u'g'r'$	6.11	335	1.0–1.6
2010 Jan 07	SDSS 1501	WHT+UCAM	55204.213149(3)	24718	0.78–1.12	$u'g'r'$	3.97	435	1.4–4.0
2010 Jan 07	SDSS 1501	WHT+UCAM	55204.270000(3)	24719	0.88–1.13	$u'g'r'$	3.97	321	1.4–3.0

and is clearly visible in Fig. 2. The flickering is reduced between phases corresponding to the white dwarf ingress and bright spot egress, indicating the source of the flickering is the inner disc and/or bright spot. Due to the heavy flickering, we decided to fit each night individually rather than fit to a phase-folded average, in order to provide a more robust estimation of our uncertainties. Our 2010 observations are discussed in section 3.4.1.

3.2.2 CTCV J2354-4700

Fig. 1 (middle) shows all of the observed eclipses from the 2007 data set of CTCV 2354 folded on orbital phase in the g' band. The white dwarf ingress and egress features are clearly visible and along with the accretion disc dominate the shape of the light curve. A weak bright spot ingress feature is visible at an orbital phase of 0.995, however the system suffers from heavy flickering, making it difficult to identify the bright spot egress. The shape of the average light curve indicates possible egress features at phases 1.060 and 1.080, but given the scatter we cannot be certain whether these represent genuine egress features or merely heavy flickering. The flickering is reduced between phases corresponding to the white dwarf ingress and egress, indicating the source of the flickering is the inner disc. Our observations from 2009 and 2010 are discussed in section 3.4.2.

3.2.3 SDSS J1152+4049

Fig. 1 (bottom) shows all of the observed eclipses from the 2010 data set of SDSS 1152 folded on orbital phase in the g' band. The signal-to-noise ratio of our data is low in comparison to other systems, but we still see a clear bright spot ingress feature at phase 0.975 in addition to a clear bright spot egress feature at phase 1.075. The white dwarf features are clear, and dominate the overall shape of the light curve. Like CTCV 1300, the eclipse of the accretion disc is difficult to discern by eye, which again suggests that the accretion disc contributes little light to this system.

3.3 Light curve modelling

To determine the system parameters we used a physical model of the binary system to calculate eclipse light curves for the white dwarf, bright spot, accretion disc and donor. Feline et al. (2004b) showed that this method gives a more robust determination of the system parameters in the presence of flickering than the derivative method of Wood et al. (1986). The model itself is based on the techniques developed by Wood et al. (1985) and Horne et al. (1994), and is an adapted version of the one used by Littlefair et al. (2008). This model relies on three critical assumptions: the bright spot lies on the ballistic trajectory from the donor star, the donor fills its Roche lobe, and the white dwarf is accurately described by a theoretical mass-radius relation.

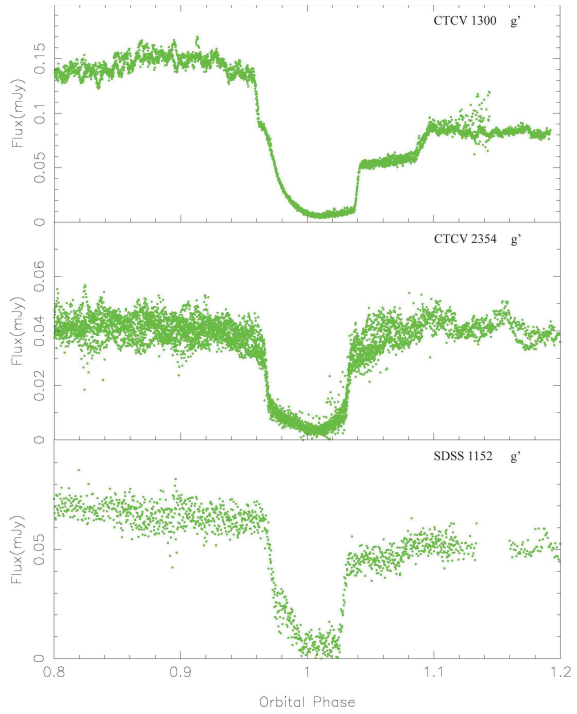

Figure 1. ULTRACAM g' band light curves of CTCV 1300 (2007, top), CTCV 2354 (2007, middle) and SDSS 1152 (2010, bottom).

Obviously these assumptions cannot be tested directly, but it has been shown that the masses derived with this model are consistent with other methods commonly employed in CVs over a range of orbital periods (e.g. Feline et al. 2004b; Tulloch et al. 2009; Copperwheat et al. 2010). The model used by Littlefair et al. (2008) had to be adapted due to the prominent bright spot observed in CTCV 1300 (Fig. 1). The 'old' model fails to correctly model the bright spot ingress and egress features in this system satisfactorily and results in a poor fit. We have thus adapted the model to account for a more complex bright spot by adding four new parameters, following Copperwheat et al. (2010), bringing the total number of variables to 14. These are:

(i) The mass ratio, $q = M_r/M_w$.
(ii) The white dwarf eclipse phase full-width at half-depth, $\Delta\phi$.
(iii) The outer disc radius, R_d/a, where a is the binary separation.
(iv) The white dwarf limb-darkening coefficient, U_w.
(v) The white dwarf radius, R_w/a.
(vi) The bright-spot scale, S/a. The bright spot is modelled as two linear strips passing through the intersection of the gas stream and disc. One strip is isotropic, while the other beams in a given direction. Both strips occupy the same physical space. The intensity distribution is given by $(X/S)^Y e^{-(X/S)^Z}$, where X is the distance along the strips. The non-isotropic strip does not beam perpendicular to its surface. Instead the beaming direction is defined by two angles, θ_{tilt} and θ_{yaw}.
(vii) The first exponent, Y, of the bright spot intensity distribution.
(viii) The second exponent, Z, of the bright spot intensity distribution.
(ix) The bright-spot angle, θ_{az}, measured relative to the line joining the white dwarf and the secondary star. This allows adjustment of the phase of the orbital hump.
(x) The tilt angle, θ_{tilt}, that defines the beaming direction of the non-isotropic strip. This angle is measured out of the plane of the disc, such that $\theta_{tilt} = 0$ would beam light perpendicular to the plane of the disc.
(xi) The yaw angle, θ_{yaw}. This angle also defines the beaming direction of the non-isotropic strip, but in the plane of the disc and with respect to the first strip.
(xii) The fraction of bright spot light that is isotropic, f_{iso}.
(xiii) The disc exponent, b, describing the power law of the radial intensity distribution of the disc.
(xiv) A phase offset, ϕ_0.

The data are not good enough to determine the white dwarf limb-darkening coefficient, U_w, accurately. To find an appropriate limb-darkening coefficient, we follow the procedure outlined in Littlefair et al. (2007), whereby an estimate of the white dwarf effective temperature and mass is obtained from a first iteration of the fitting process outlined below, assuming a limb-darkening coefficient of 0.345. Littlefair et al. (2007) show that typical uncertainties in U_w are $\sim 5\%$, which leads to uncertainties in R_w/a of $\sim 1\%$. These errors have negligible impact on our final system parameters.

As well as the parameters described above, the model also provides an estimate of the flux contribution from the white dwarf, bright spot, accretion disc and donor. The white dwarf temperature and distance are found by fitting the white dwarf fluxes from our model to the predictions of white dwarf model atmospheres (Bergeron et al. 1995), as shown in Fig. 3. We find that with the exception of CTCV 2354, all of the systems analysed lie near, or within, the range of white dwarf colours allowed by the atmosphere models of Bergeron et al. (1995), although the systems do not always lie near the track for the appropriate mass and radius of the white dwarf. Littlefair et al. (2008) compare the temperatures derived using light curve fits to those found using SDSS spectra and GALEX (Galaxy Evolution Explorer) fluxes for a small number of systems and conclude their white dwarf temperatures are accurate to ∼1000K. The systems examined by Littlefair et al. (2008) are all found to lie close to the Bergeron tracks; it is likely that systems that lie far from the tracks are less accurate. We note our temperatures have larger uncertainties than those of Littlefair et al. (2008). This is because our temperatures take into account the uncertainty in white dwarf mass when comparing the white dwarf fluxes to the models of Bergeron et al. (1995).

It is possible that our white dwarf colours are affected by contamination from the disc or bright spot, or an unmodelled light source such as a boundary layer. If our white dwarf colours are incorrect, then our derived white dwarf temperatures will be affected. Changing the white dwarf temperature will alter U_w. Our model fitting measures R_w/a and uses a mass-radius relationship to infer M_w, which is then used to find the mass of the donor star. However, U_w and R_w are partially degenerate, so U_w therefore affects R_w and M_w. M_w is also affected by temperature changes because the white dwarf mass-radius relationship is temperature dependent. The white dwarf temperature also affects

the luminosity of the system, and hence distance estimate. It is therefore important to quantify the effect that incorrect white dwarf temperatures may have on distance estimates and our final derived system parameters. To do this, we altered the white dwarf temperature by 2000K and performed the fitting procedure described above on our best quality, white-dwarf dominated systems. For lower quality data, the random errors dominate over any systematic errors, and thus changes to the best quality data represent a worst case scenario. We find that changing the white dwarf temperature by 2000K changes R_w/a by less than 1σ. The white dwarf distance estimates change by 10-20pc. We therefore conclude any error in white dwarf temperature that may occur does not affect our final system parameters by a significant amount. We note here that our moedelling does not include treatment of any boundary layer around the white dwarf, and assumes all of the white dwarf's surface is visible. Either effect could lead to systematic uncertainty in our white dwarf radii (Wood et al. 1986).

A Markov Chain Monte Carlo (MCMC) analysis was used to adjust all parameters bar U_W. MCMC analysis is an ideal tool as not only does it provide a robust method for quantifying the uncertainties in the various system parameters, it is more likely to converge on the global minimum χ^2 rather than a local minimum χ^2. We refer the reader to Ford (2006), Gregory (2007) and references therein for excellent overviews of MCMC chains and Bayesian statistics and limit ourselves to a simple overview.

MCMC is a random walk process where at each step in the chain we draw a set of model parameters from a normal, multi-variate distribution. This is governed by a covariance array, which we estimate from the initial stages of the MCMC chain. The step is either accepted or rejected based on a transition probability, which is a function of the change in χ^2. We adopt a transition probability given by the Metropolis-Hastings (M-H) rule, that is $P = \exp^{-\Delta\chi^2/2}$. The sizes of the steps in the MCMC chain are multiplied by a scale factor, tuned to keep the acceptance rate near 0.23, which is found to be the optimal value for multi-variate chains such as these (Roberts et al. 1997).

A typical MCMC chain included some 700,000 steps, split into two, 350,000 step sections. The first section is used to converge *towards* the global minimum and estimate the covariance matrix (known as the burn-in phase). The second section fine tunes the solution by sampling areas of parameter space around the minimum. In doing so, we also produce a robust estimation of our uncertainties. Together, these steps are usually sufficient to enable the model to converge on the statistical best fit, regardless of the initial starting parameters.

While implementing the MCMC code, we discovered a bug in our original code. The re-binning code used to average several light curves together mistreated the widths of the bins, which in turn affected the trapezoidal integration of the model over these bins. The direct result was that in cases of heavy binning, such as systems with heavy flickering or where several light curves had been averaged together (e.g. SDSS 1502), the white dwarf radius, R_w/a, was underestimated. The exact amount depended on the level of binning used. This consequently resulted in an overestimate of the white dwarf mass. Since the mass of the donor star, M_r, is related to the white dwarf mass M_w by $M_r = qM_w$, we were also left with an overestimate of the donor mass. This problem affects all of our previously published eclipsing-CV papers (Feline et al. 2004a, 2004b; Littlefair et al. 2006a, 2006b, 2007, 2008) by differing amounts. However, in most cases re-modelling provides new system parameters that are within $1-2\sigma$ of our original results, with only two exceptions (see section 3.4). The new results are presented in Table 3.

For each system we ran an MCMC simulation on each phase-folded u', g', r' or i' light curve from an arbitrary starting position. Exceptions include CTCV 1300, where each night of observations was fit individually, and SDSS 1152 and SDSS 1501, for which we only calculated fits in the g' and r' bands due to u'-band data of insufficient quality to constrain the model. Where no u' band MCMC fit could be obtained, we fit and scaled the g' band model to the u' band light curves without χ^2 optimisation. This allows us to estimate the white dwarf flux in the u' band, and thus estimate the white dwarf temperature. In the case of SDSS 1501, we also fit a different data set to the 2006 WHT data of Littlefair et al. (2008). We fit our model to the single light curve dated 2004 May 17. This 2004 data was not fit by Littlefair et al. (2008) as the simplex methods used gave a seemingly good fit to the 2006 data. Despite appearing to have converged to a good fit, the MCMC analysis revealed that the 2006 data does not constrain the model, most likely due to the very weak bright spot features. The 2004 data shows much clearer and well-defined bright-spot features than the 2006 data (see Fig.1 of Littlefair et al. 2008), and so despite only having one eclipse (and thus lower signal-to-noise) it is favoured for the fitting process. In general our fits to each system are in excellent agreement with the light curves (see Fig. 2), giving us confidence that our new models accurately describe each system.

To obtain final system parameters we combine our MCMC chains with Kepler's 3^{rd} law, the orbital period, our derived white dwarf temperature, and a series of white dwarf mass-radius relationships. We favour the relationships of Wood (1995), because they have thicker hydrogen layers which may be more appropriate for CVs. However, they do not reach high enough masses for some of our systems. Above $M_w = 1.0M_\odot$, we adopt the mass-radius relationships of Panei et al. (2000). In turn, these models do not extend beyond $M_w = 1.2M_\odot$; above this mass we use the Hamada & Salpeter (1961) relationship. No attempt is made to remove discontinuities from the resulting mass-radius relationship.

We calculate the mass ratio q, white dwarf mass $M_w/M_\odot$, white dwarf radius $R_w/R_\odot$, donor mass $M_r/M_\odot$, donor radius $R_r/R_\odot$, inclination i, binary separation $a/R_\odot$ and radial velocities of the white dwarf and donor star (K_w and K_r, respectively) for each step of the MCMC chain. Since each step of the MCMC has already been accepted or rejected based upon the Metropolis-Hastings rule, the distribution function for each parameter gives an estimate of the probability density function (PDF) of that parameter, given the constraints of our eclipse data. We can then combine the PDFs obtained in each band fit into the total PDF for each system, as shown in Fig. 4. We note that most systems have system parameters with a Gaussian distribution with very little asymmetry. Our adopted value for a given parameter is taken from the peak of the PDF. Upper and lower error bounds are derived from the 67% confidence levels. For sim-

plicity, since the distributions are mostly symmetrical, we take an average of the upper and lower error bounds. The final adopted system parameters are shown in Table 3, although Fig. 7 and 8 show the true 67% confidence levels for the white dwarf mass and donor mass respectively, for each system.

3.4 Notes on individual systems

3.4.1 CTCV 1300

As noted in section 3.3, the two eclipses of CTCV 1300 were modelled individually due to the heavy pre-eclipse flickering present in each light curve. The $u'g'r'$ eclipses from the night of 2007 June 10 gave consistent results, as did the $u'g'i'$ eclipses from the night of 2007 June 13. However, results from the individual nights were not consistent with each other, and we are presented with two distinct solutions which are the result of heavy pre-eclipse flickering altering the shape of the bright spot ingress feature. This in turn gives two very different values for the mass ratio, q. Encouragingly we find our white dwarf masses and radii are consistent between nights. To derive the final system parameters we use the PDFs as outlined in section 3.3 and then take an average of the solution from each night. The error is taken as the standard deviation between the two values.

In Fig. 5 we see a g'-band eclipse from June 2010 together with a modified version of the model obtained from the 2007 dataset. This new model is found by starting from an average of the two 2007 fits and using a downhill simplex method to vary all parameters bar q, $\Delta\phi$, R_w/a and U_w. These parameters should not change with time, and so the simplex fit will confirm if our bright spot positions and white dwarf dwarf radius are correct, and thus if our system parameters are reliable. We use a simplex method for two reasons; firstly since we are performing a consistency check and are not extracting system parameters from the fitting process we do not require a full MCMC analysis. Secondly, the bright spot flux appears to have reduced significantly, and the strength of the bright spot ingress feature means that we cannot constrain a full fit using the MCMC model used previously. The model confirms the bright spot flux has decreased considerably, although an orbital hump is still visible. The white dwarf flux remains almost unchanged, although the disc appears brighter. The fit to the data is good, indicating that the models derived from the 2007 data (and used to derive our system parameters) are reliable.

3.4.2 CTCV 2354

In section 3.2.2 we noted that the shape of the light curve in Fig. 1 indicated possible bright spot egress features around phases 1.060 and 1.080. Fig. 2 shows that our model has fit the bright spot egress feature at phase 1.080. Given the strength and shape of the bright spot features and general scatter present in the light curve we cannot be certain if the bright spot positions have been correctly identified by our model, and thus there is some element of doubt as to the value obtained for our mass ratio and thus donor mass. It is at this point we draw the readers attention to our 2010 data, shown in Fig. 6. The eclipse dated 2010 May 3 (centre panel) shows clear bright spot ingress and egress features, with a

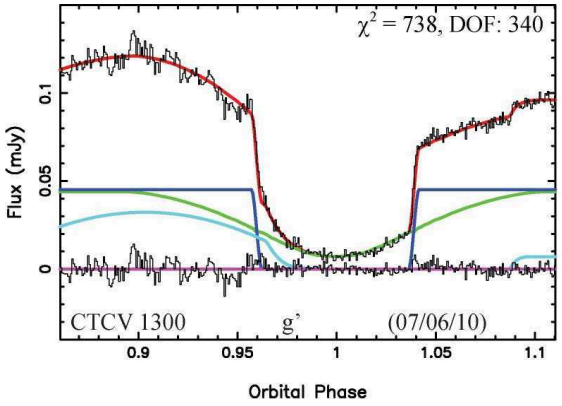

Figure 5. Our June 2010 g' band eclipse of CTCV 1300, together with a modified model found using the 2007 data. Starting from an average of the two 2007 models, we ran a downhill simplex fit varying all parameters bar q, $\Delta\phi$, R_w/a and U_w.

clear orbital hump visible from phases 0.70–0.95. The system is much brighter in this state than the 2007 data previously modelled, in part due to a dramatic increase in bright spot flux. As with CTCV 1300 we carried out a downhill simplex method to vary all parameters bar q, $\Delta\phi$, R_w/a and U_w. Our fit to the eclipse of May 3 is especially pleasing, as its excellent agreement with the light curve confirms that our 2007 model correctly identified the bright spot egress feature and thus the mass ratio obtained is reliable.

Fig. 6 also shows a single eclipse observed just one month later (June 2010, right panel), and six eclipses averaged together from June 2009 (left panel). Both of these datasets are fit with a downhill simplex model as above. The June 2009 and June 2010 datasets are in stark contrast to the May 2010 data, with the bright spot features appearing extremely faint (2009), or seemingly non-existent (June 2010). The disc flux in the June 2010 data appears to have increased significantly, giving rise to a distinct "u" shape. The rapid change in bright spot and disc light curves over such short (1 month - 1 year) time scales suggests that the disc is highly unstable.

3.4.3 DV UMa

Our donor mass derived for DV UMa has increased by 6.1σ (ΔM=0.039$M_\odot$) from that published by Feline et al. (2004b). Close inspection of the original fit reveals that the bright spot features are fit poorly by the old bright spot model. This arises because the old bright spot model could not describe the complex bright spot profile present and an innacurate value of the mass ratio is found as a result. Our new bright spot model is much better in this respect, and is able to take into account a wider variety of geometric effects and orientations. Given that our white dwarf radius is consistent with that of Feline et al. (2004b), this seems the most likely cause of such a large change. It is worth noting that our new donor masses for both DV UMa and XZ Eri, are both consistent with the masses obtained by Feline et al. (2004b) using the derivative method, which, unlike our parameterised model, does not make any attempt to recreate the bright spot eclipse profile (e.g. Wood et al. 1986; Horne et al. 1994; Feline et al. 2004a; Feline et al. 2004b).

Table 3 (system parameters) goes here (landscape). See separate file (table3params).

Table 3.

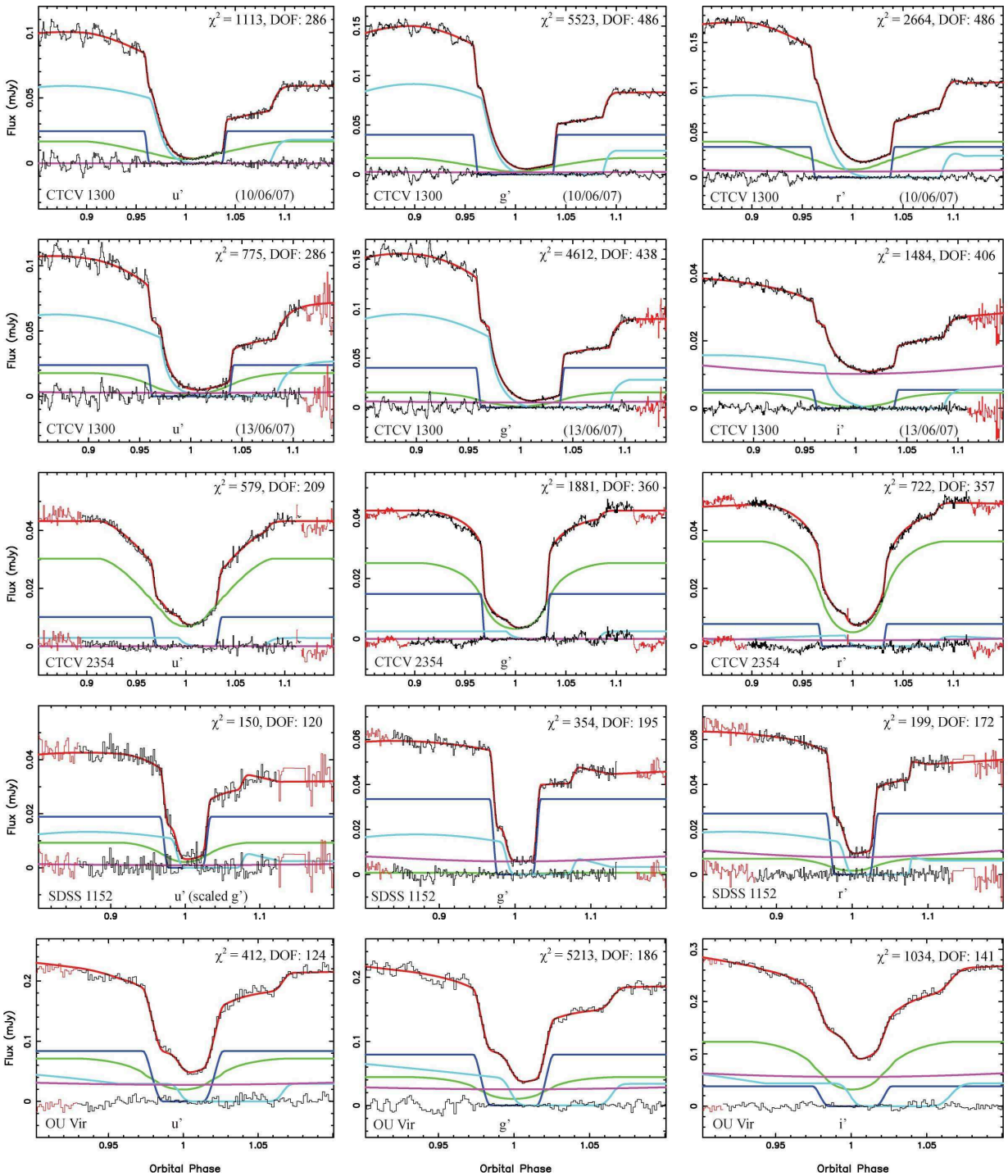

Figure 2. The phased-folded $u'g'r'$ or $u'g'i'$ light curves of the CVs listed in Table 3, fitted using the model outlined in section 3.3. The data (black) are shown with the fit (red) overlaid and the residuals plotted below (black). Below are the separate light curves of the white dwarf (dark blue), bright spot (light blue), accretion disc (green) and the secondary star (purple). Data points omitted from the fit are shown in red. χ^2 values for each fit, together with the number of degrees of freedom (DOF) are also shown.

3.4.4 SDSS 1502

Our new fits to SDSS 1502 decrease the donor mass by 2.9σ ($\Delta M_r = 0.012 M_\odot$) from that of Littlefair et al. (2008). Our mass ratio and inclination are consistent with those of Littlefair et al. (2008), however our white dwarf radius, R_w, has increased by 13 percent (3.4σ). We believe the primary reason for this change was that the original fit was heavily binned, and thus more susceptible to the bug outlined in section 3.3.

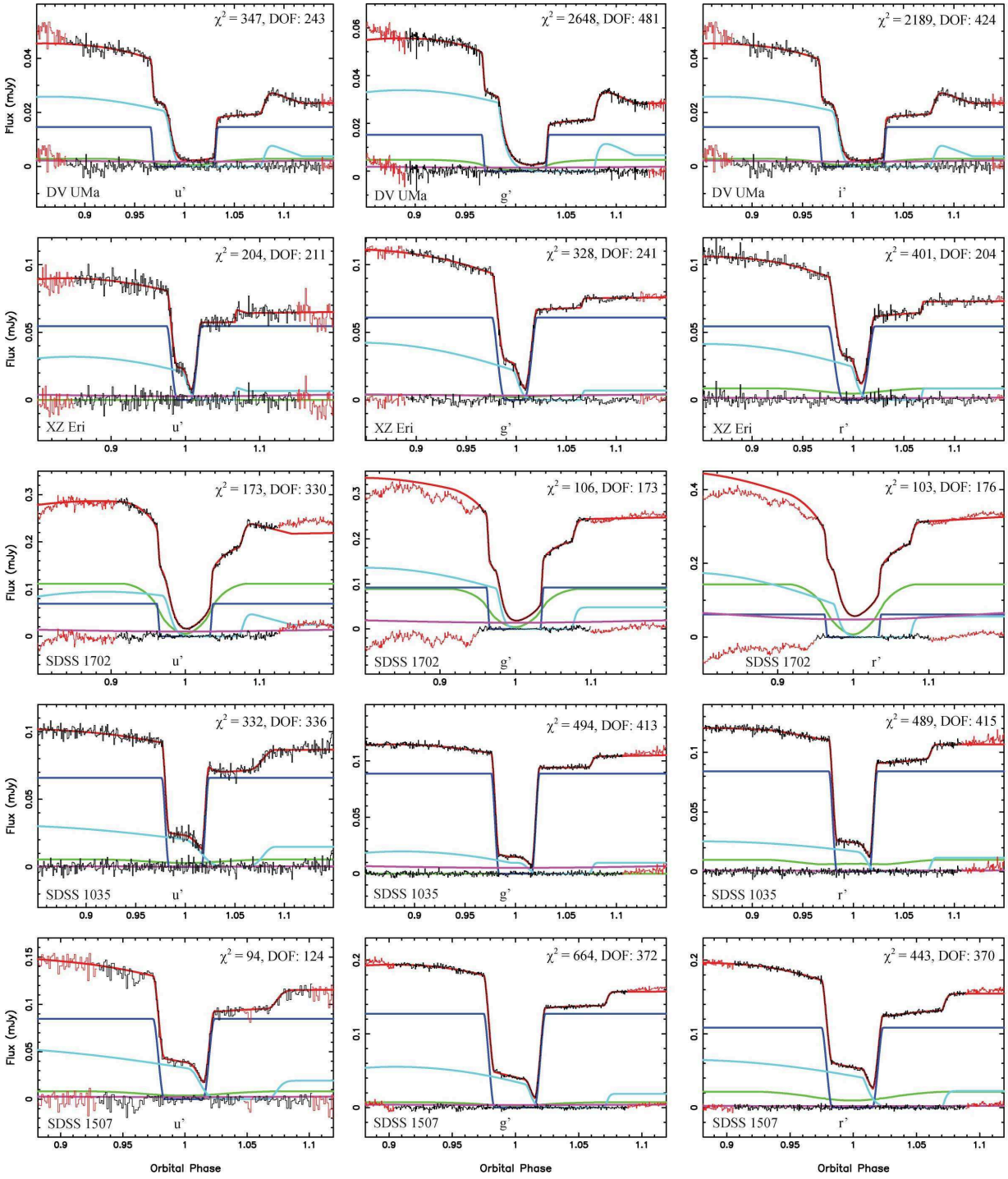

Figure 2 – *continued*

3.4.5 SDSS 1501

The most important change of all of our re-modelled systems is for that of SDSS 1501. Whilst our donor mass has only increased by 1.9σ from that of Littlefair et al. (2008), we note that our uncertainties are large ($\sigma M_r = 0.010 M_\odot$) and the mass difference is large enough to take this system from being a post-period-bounce system, to a pre-period-bounce system. Although our errors do not formally rule out the possibility of SDSS 1501 being post-period-bounce, the donor's position with respect to the evolutionary tracks shown in Fig. 8 strongly favours that of a pre-period-bounce system. Such a change arises from a difference in bright spot positions between our model and that of Littlefair et al. (2008), which in turn affect the mass ratio obtained. The data used by Littlefair et al. (2008) shows a very weak bright spot ingress feature. With the improvements made to the modelling process resulting from the introduction of MCMC,

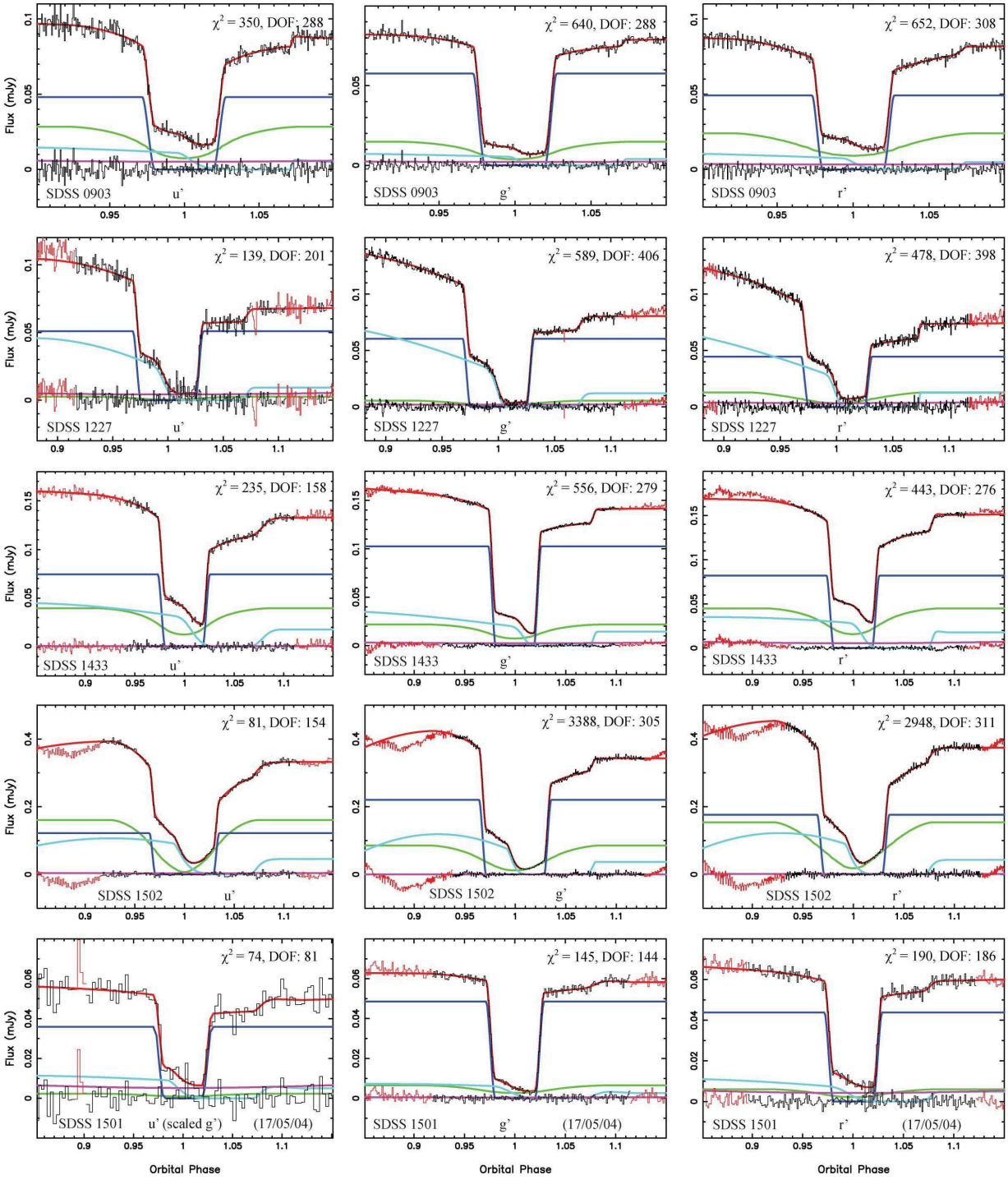

Figure 2 – *continued*

it is clear that the 2006 data used by Littlefair et al. (2008) does not constrain the mass ratio, q, tightly enough. In contrast, the 2004 data shows much clearer bright spot features, and we therefore favour this over the 2006 data as discussed in section 3.3.

4 DISCUSSION

4.1 White dwarf masses

Population studies by Willems et al. (2005) predict that between 40 and 80 percent of CVs are born with He-core white dwarfs ($M_w \lesssim 0.50 M_\odot$) and therefore He-core white dwarfs (He-WDs) are expected to be common amongst CV primaries. It is surprising then that out of our sample of 14 systems, we observe no He-WDs. Of all of our objects,

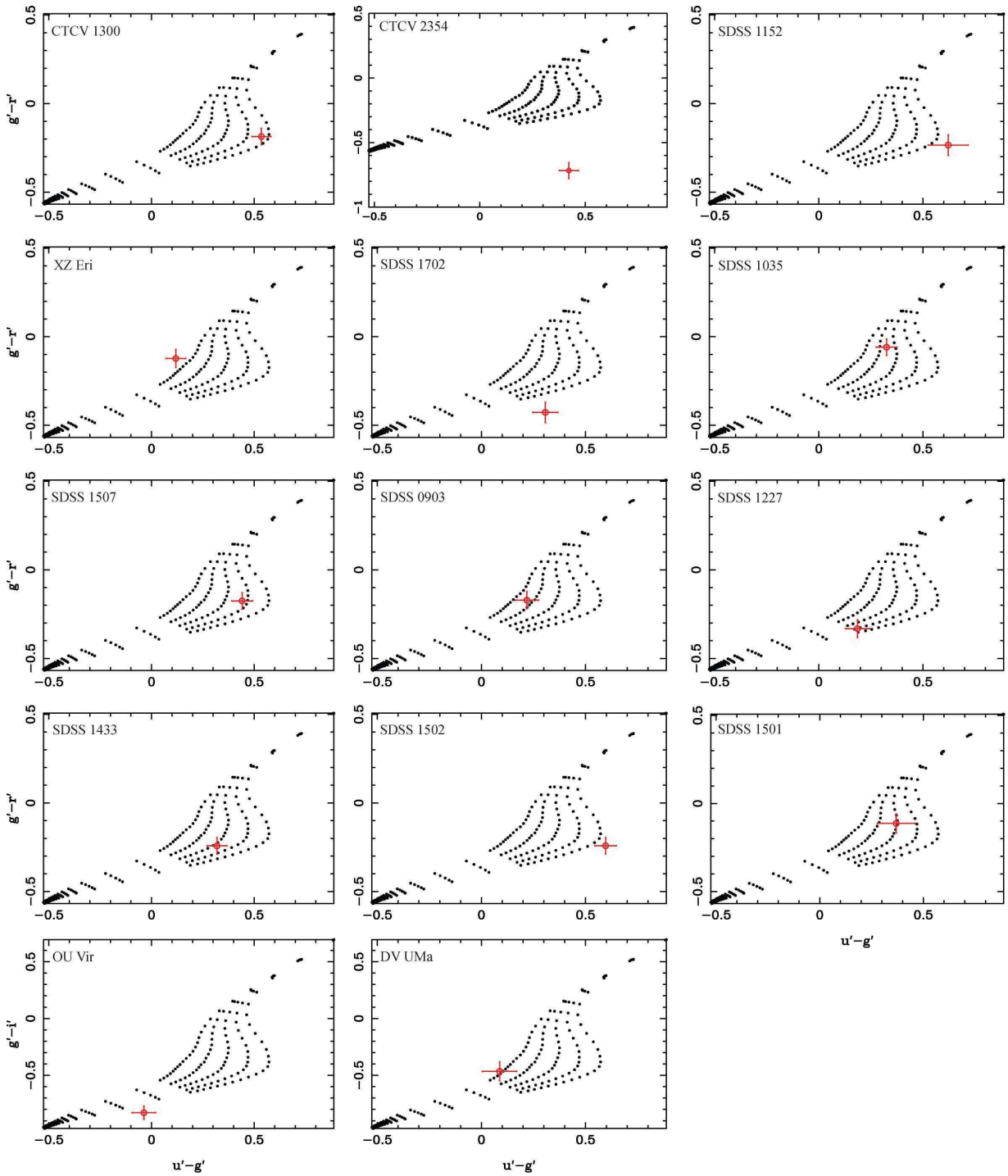

Figure 3. The white dwarf colours derived from our model fitted together with the white dwarf models of Bergeron et al. (1995). From top to bottom, each curve represents log g = 9.0, 8.5, 8.0, 7.5 and 7.0 respectively. The measured white dwarf colours are shown here in red, and are used to derive the white dwarf temperature, which in turn is used to correct the white dwarf mass-radius relationships used later to obtain the final system parameters.

SDSS 1152 is found to have to the lowest white dwarf mass with $M_w = 0.560 \pm 0.028$. The mass distribution of Kepler et al. (2007) for SDSS white dwarfs suggests He-WDs have a typical mass of $\sim 0.38 M_{\odot}$. The most massive He-WDs are thought to form from single RGB stars, which due to extreme mass loss are able to avoid the Helium flash; D'Cruz et al. (1996) consider models with a range of mass loss rates on the RGB and manage to produce He-WDs with masses up to $\sim 0.48 M_{\odot}$. It is likely that this represents an upper limit to the mass of He-WDs and hence SDSS 1152 is too massive to be a viable candidate for a He-core white dwarf.

We find that our white dwarf masses are not only too massive to be He-WDs, but are also well in excess of the aver-

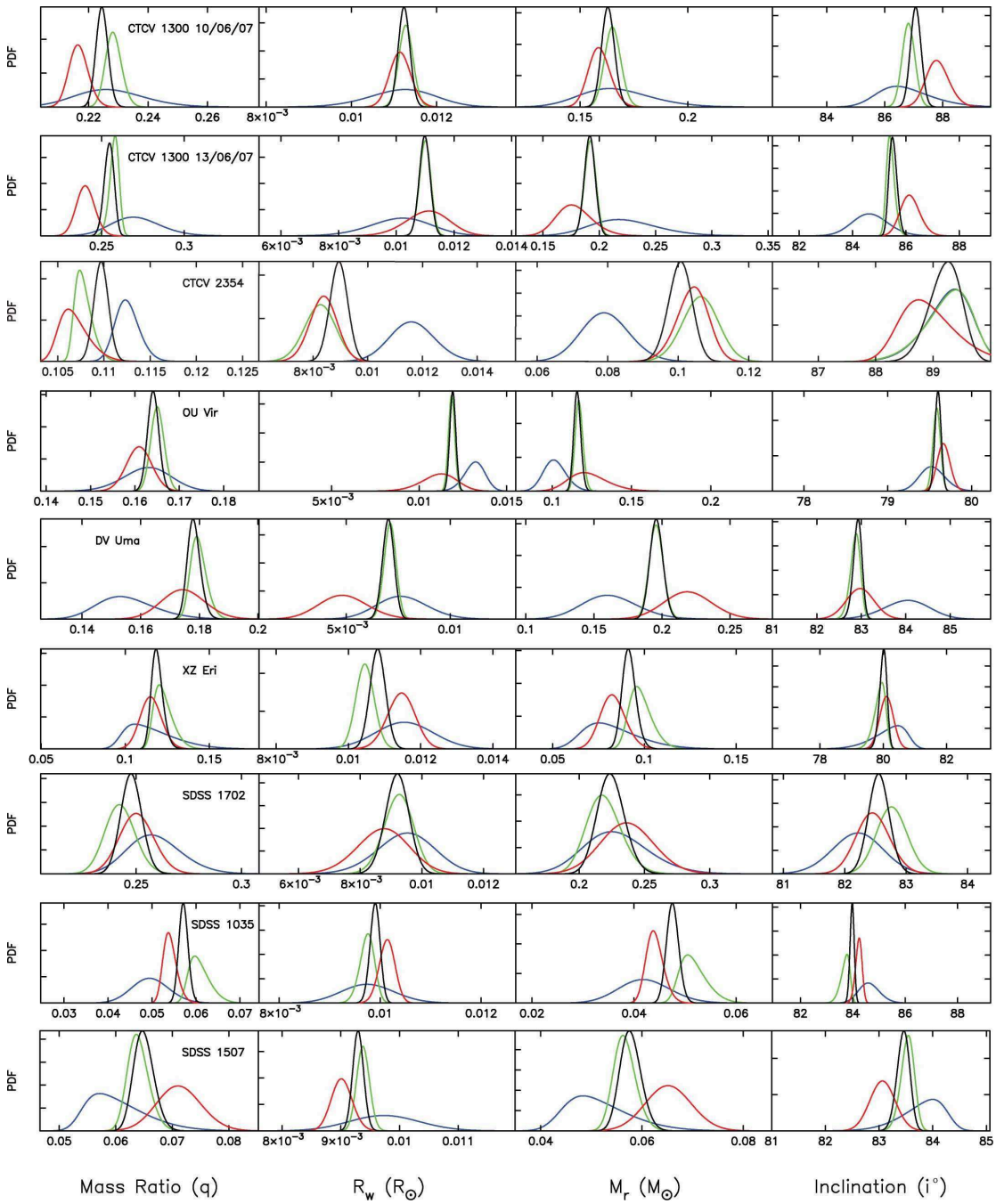

Figure 4. The normalised probability density functions for each system, derived using the MCMC chains, orbital period and the mass–radius relationships of Wood (1995), Panei et al. (2000) and Hamada & Salpeter (1961), at the appropriate white dwarf temperature. The red curve represents the r' or i' band fit, the green represents the g' band, and blue curve (where present) represents the u' band. The black represents the total, combined PDF. Shown are the PDFs for mass ratio q, white dwarf radius $R_w/R_\odot$, donor mass $M_r/M_\odot$, and inclination i°.

age mass for single DA white dwarfs. Using the same method as Knigge (2006), we calculated the average white dwarf mass of our entire sample to be $M_w = 0.81 \pm 0.04 M_\odot$, with an intrinsic scatter of $0.13 M_\odot$. In comparison, Liebert et al. (2005) find the mean mass of DA white dwarfs to be $M_w \sim 0.603\ M_\odot$, while Kepler et al. (2007) find a mean mass of $M_w = 0.593 \pm 0.016 M_\odot$.

Our study thus supports previous findings (e.g. Warner 1973, 1976; Ritter 1976, 1985; Robinson 1976; Smith & Dhillon 1998; Knigge 2006) that white dwarfs in CVs are on average much higher in mass than single field stars. Like Littlefair et al. (2008), we compare our masses to the average mass of $M_w = 0.73 \pm 0.05 M_\odot$ for white dwarfs in CVs below the period gap (Knigge 2006) and find that our white dwarf masses are generally much higher. This is especially so for systems $P_{orb} \leqslant 95$ mins, where we find a mean white dwarf mass of $M_w = 0.83 \pm 0.02 M_\odot$, with an intrinsic scatter of $0.07 M_\odot$. Some our white dwarf masses

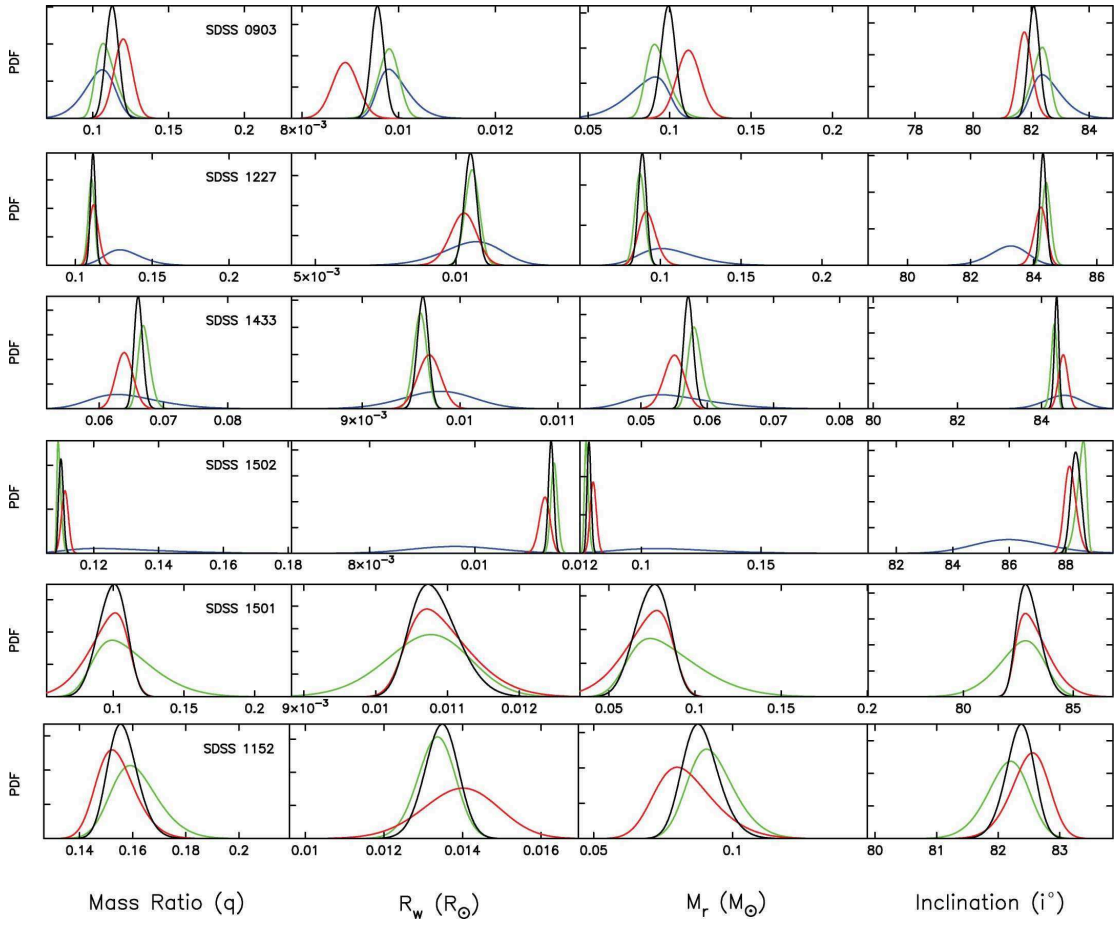

Figure 4 – *continued*

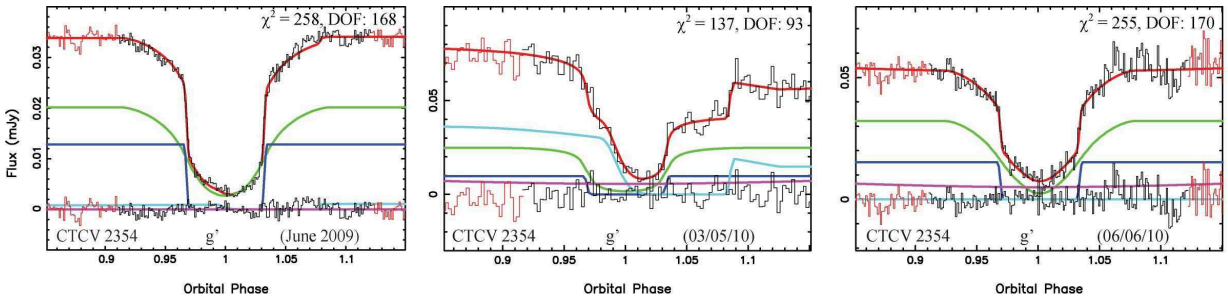

Figure 6. Our g' band observations of CTCV 2354 from 2009 (left), 2010 May 3 (centre) and 2010 June 6 (right), fit with a modified version of the model obtained from the 2007 data as described in section 3.4.2.

are revised, and have accordingly moved downwards in mass compared to Littlefair et al. (2008), but as Fig. 7 shows, for $P_{orb} \leqslant 95$ mins, 8 out of 9 systems are more massive than the average found by Knigge (2006), with SDSS 1502 the only exception. On the same plot, we also plot the dispersion of masses as found by Knigge (2006) and the mean mass of single SDSS white dwarfs found by Kepler et al. (2007). Note that the Knigge (2006) sample contains three systems also included in our study: OU Vir, DV UMa and XZ Eri, using the old mass determinations of Feline et al. (2004a, 2004b). We see most of our masses are within the dispersion found, indicating that no individual white dwarf mass is unusual. However 8 out of 9 systems above average does seem anomalously high, considering that if we model the white dwarf masses as a Gaussian distribution, the probability of such an occurrence is less than 2 percent (independent of the actual mean or variance). Such difference between our sample and that of Knigge (2006) is concerning, and it is therefore desirable to consider the selection effects, considering the majority of our short period systems are all SDSS objects (Szkody et al. 2004, 2005, 2006, 2007).

The majority of SDSS CVs found are generally rejected quasar candidates with a limiting magnitude of $g' = 19-20$, and are initially selected for follow up on the basis of u'-g' colour cuts (see Gänsicke et al. (2009) for a more in depth description). Littlefair et al. (2008) show that systems with

$M_w \geqslant 0.50 M_\odot$ are blue enough to pass the SDSS colour cuts and conclude that selection effects such as these are unlikely to explain the high mass bias of our white dwarf sample. However, the majority of the systems we have studied are close ($g' \sim 17.5 - 19.5$) to the $g' = 19$ limit of the SDSS survey. This raises the possibility that the SDSS sample only finds the brightest of the short period CVs. Ritter & Burkert (1986) have shown that CVs with high mass white dwarfs are brighter than their low mass counterparts. This suggests there maybe some bias towards high mass dwarfs. However, this conclusion is not appropriate to the systems studied here: Ritter & Burkert (1986) only consider the effects of accretion luminosity whereas in most of our systems the white dwarf considerably outshines the accretion disc.

Zorotovic et al. (2011) consider selection effects in white dwarf dominated SDSS systems with a variety of different mass transfer rates and conclude there is actually bias *against* high mass white dwarfs. They find a $0.90 M_\odot$ white dwarf is approximately 0.15 magnitudes fainter than a $0.75 M_\odot$ white dwarf, which corresponds to a decreased detection efficiency of $\sim 20\%$. This suggests that our finding of high mass white dwarfs at short orbital periods is not due to selection effects, and is in fact a true representation of the intrinsic mass distribution of CVs. However, this analysis only considers white dwarf luminosity; in some of our systems the bright spot features are prominent, and contribute significantly to the overall flux of the system. It remains possible that the finding of very high white dwarf masses for our short period CVs is due to selection effects. However, a full and thorough quantification of any bias would require detailed calculations of the luminosity of white-dwarf dominated systems (including bright spot emission) plus an investigation of the selection effects in the SDSS sample. Such an analysis is beyond the scope of this paper.

Our results have important consequences for the modelling of nova outbursts and their impact on the long-term evolution on CVs. Typical calculations show that the mass of the white dwarf decreases by between 1 and 5 percent per 1000 nova cycles (e.g. Yaron et al. 2005; Epelstain et al. 2007). The dominance of high-mass white dwarfs in our sample of short period systems suggests that any white dwarf erosion due to nova explosions must be minimal, or that not all of the accreted matter is ejected during nova ignition, resulting in the white dwarf mass *increasing* over time. This could, in principle enable the white dwarfs in cataclysmic variables to grow in mass until they reach the Chandrasekhar limit.

4.2 Period bounce

Population synthesis models for cataclysmic variables (e.g. Kolb 1993; Willems et al. 2005) all predict that large numbers of the CV population ($\sim$15 - 70 percent) have evolved past the period minimum. This has always been in stark contrast to observations, possibly in part due to selection effects (e.g. Littlefair et al. 2003).

Littlefair et al. (2006b, 2007, 2008) identified four systems (SDSS 1035, SDSS 1507, SDSS 1433, SDSS 1501) with donors below the sub-stellar limit, three of which are likely to be post-period-bounce CVs (SDSS 1035, SDSS 1501 and SDSS 1433). Our subsequent re-analysis gives three systems (SDSS 1035, SDSS 1507, SDSS 1433) with donors below the sub-stellar limit, two of which (for reasons outlined below) we believe are post-period-bounce CVs (SDSS 1035 and SDSS 1433). SDSS 1501, which no longer features as a post-period-bounce system, is discussed in greater detail in section 3.4.5.

Sirotkin & Kim (2010) claim that SDSS 1433 cannot be considered a post-period-bounce object since the mass transfer rates and donor star temperatures implied are too high. The mass transfer rate is found using an estimate of the white dwarf temperature (Townsley & Gänsicke 2009), while the donor star temperature is inferred using a semi-empirical relationship that is also dependent on the white dwarf temperature. The white dwarf temperature used by Sirotkin & Kim (2010) is that derived by Littlefair et al. (2008) from model fitting. We believe, at least in this case, that using $\dot{M}$ and T_2 is an unreliable test of the evolutionary status of CVs donors, since accurate determinations of the white dwarf temperature are difficult to obtain. Of all the system parameters we have derived, the white dwarf temperatures are the least well constrained, and this does not take into account systematic errors. Since the white dwarf temperature is found using the flux from just three colours, and our model does not include all possible sources of luminosity (e.g. a boundary layer), there is a good chance our white dwarf temperatures are affected by systematic errors at some level, as discussed in section 3.3. Instead, we focus on the donor star mass, M_r.

If the angular momentum loss rate is similar for systems with identical system parameters, we expect all CVs to follow very similar evolutionary tracks with a single locus in the mass-period relationship (and by analogy, mass-radius relationship) for CV donors, as shown in Fig. 8. The empirical donor star mass-radius relationship derived by Knigge (2006) shows that a single evolutionary track does very well at describing the observed $M_2 - P_{orb}$ relationship, although the shape of that relationship is poorly constrained at low masses. A single evolutionary path also explains the presence of the "period spike", a long sought after feature in the orbital period distribution recently identified by Gänsicke et al. (2009). We therefore expect there to be a unique donor mass corresponding to the minimum orbital period, below which an object becomes a period-bouncer. The exact mass at which this occurs is very uncertain, and does not necessarily correspond to the sub-stellar limit (Patterson 2009). From the empirical work of Knigge (2006), the best estimate for M_{bounce} is $M_r = 0.063 \pm 0.009 M_\odot$. Three of our systems (SDSS 1035, SDSS 1433 and SDSS 1507) fall well below this value, although SDSS 1507 is an unusual system, and is discussed in the following section. As in Littlefair et al. (2008), we do not include it in our sample of post-period minimum CVs. We therefore have two strong candidates for post-period minimum CVs (SDSS 1035 and SDSS 1433) from our total sample of 14 CVs (nine of which are SDSS systems). From this, we estimate that 14 ± 7 percent of all CVs below the period gap, and 22 ± 11 percent of all short period CVs ($P_{orb} \leqslant 95$ mins) have evolved past the period minimum. These findings are consistent, albeit to a crude approximation given our small sample of objects, with current population synthesis models. Since all of our short period systems are SDSS CVs, we cannot rule out selection effects, but Gänsicke et al. (2009) have shown that the number of period minimum CVs found within the SDSS

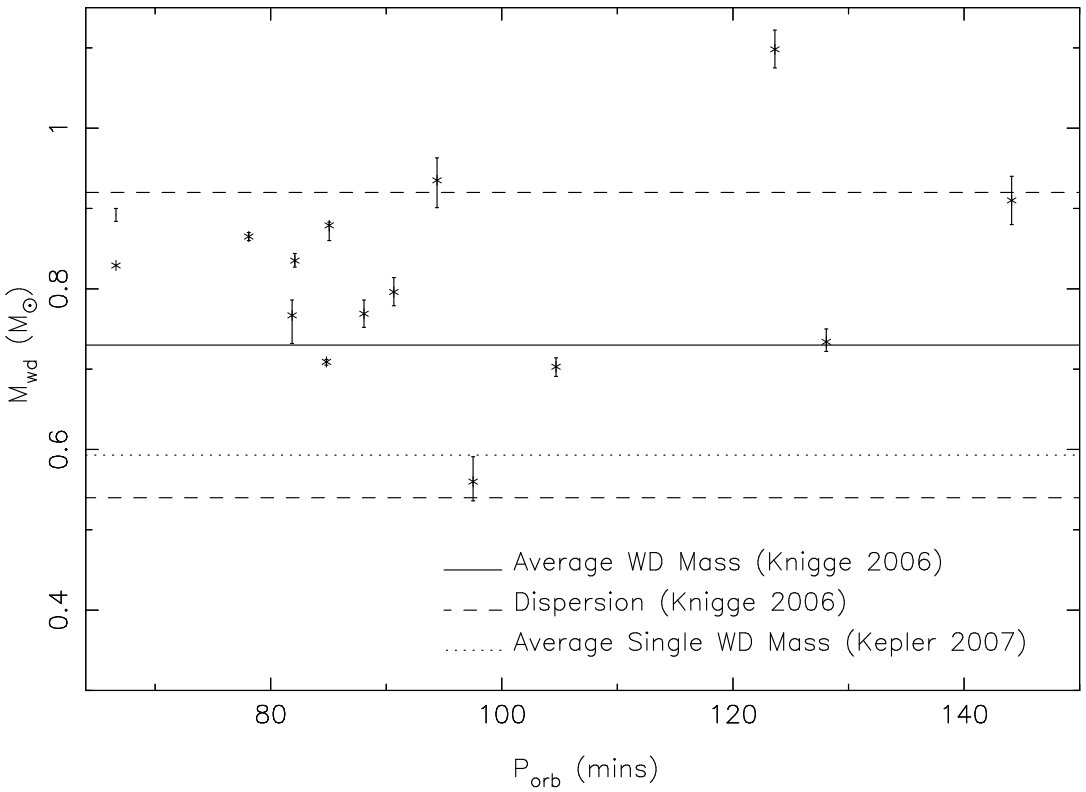

Figure 7. White dwarf mass as a function of orbital period. The mean white dwarf mass for systems below the period gap, as found by Knigge (2006) is shown with a solid line, along with the associated intrinsic scatter (dashed line). The mean white dwarf mass in single stars as found by Kepler et al. (2007) is shown by a dotted line.

is broadly consistent with other surveys, allowing for normalisation of survey volumes.

4.3 SDSS 1507

The orbital period of SDSS 1507 is far below the well-defined period minimum and thus the nature of this system is of great interest to theorists and observers. It is possible that this system represents the true orbital period minimum as predicted by Kolb & Baraffe (1999). However, if this is indeed the case, we would expect a large number of systems between orbital periods of 67 minutes, and 83 minutes where the period spike is observed (Gänsicke et al. 2009). These systems are not observed, and hence it is likely that some other mechanism is responsible. Littlefair et al. (2007) speculate that this system was either formed directly from a white dwarf/brown dwarf binary, while Patterson et al. (2008) argue that the system could be a member of the halo. Both derive system parameters, and both obtain distance estimates to the system.

Our derived system parameters are consistent with those of Littlefair et al. (2007) and Patterson et al. (2008), within uncertainties. Our distance estimate is in excellent agreement with Littlefair et al. (2007), which is not suprising since we both calculate the distance using the same methods and dataset. However, our new distance estimate still places the system nearer than that of Patterson et al. (2008). Patterson et al. (2008) obtain a lower limit to the distance using parallax. The parallax value implies a distance $d > 175$ pc, which taken alone, is consistent with our estimate of $d = 168 \pm 12$ pc. Patterson combines his parallax with a range of other observational constraints using Bayesian methods to yield a final distance estimate of $d = 230 \pm 40$ pc. If our distance of $d = 168 \pm 12$ pc is nearer the true distance, then combining with Patterson's proper motion measurement of $0.16''/yr$ yields a transverse velocity of $d = 128 \pm 9$ kms^{-1}. This lower transverse velocity is still very much an outlier in the distribution of 354 CVs shown in Fig.1 of Patterson et al. (2008). Therefore, regardless of which distance is correct, the proper motion of SDSS 1507 still supports halo membership.

4.4 Exploring the standard model of CV evolution

Fig. 8 shows the evolutionary models of Kolb & Baraffe (1999) calculated with enhanced mass-transfer rates. Also shown is a model with 50 percent star spot coverage on the surface of the donor. Positions of the period minimum, and period gap as found by Knigge (2006) are also shown. Mass determinations for all systems presented here are included. We see that the standard theoretical models are a poor fit to the data. For a given mass, the models of Kolb & Baraffe (1999) significantly underestimate the orbital period, and thus the donor radii.

Models with enhanced mass transfer rates and star spot coverage do rather better at reproducing the observed donor masses, although the general scatter of short period systems makes choosing between these difficult. This is in line with the conclusions of Littlefair et al. (2008). The models begin to diverge significantly at orbital periods greater than

100 minutes. Unfortunately, in this regime there are few systems with precisely known donor masses. Clearly, we require more mass determinations for systems with orbital periods between 100 and 130 minutes.

5 CONCLUSIONS

We present high-speed, three-colour photometry of a sample of 14 eclipsing CVs. Of these CVs, nine are short period ($P_{orb} \leqslant 95$ minutes), and one is within the period gap. For each of the 14 objects we determine the system parameters by fitting a physical model of the binary to the observed light curve by χ^2 minimisation. We find that two of our nine short period systems appear to have evolved past the period minimum, and thus supports various assertions that between 15 and 70 per cent of the CV population has evolved past the orbital period minimum. The donor star masses and radii are not consistent with model predictions, with the majority of donor stars being $\sim$10 per cent larger than predicted. Our derived masses and radii show that this can explained by either enhancing themass transfer rate or modifying the stellar physics of the donor star to take into account star spot coverage. Unfortunately, we still lack enough precise donor masses between orbital periods of 100 and 130 minutes to choose between these alternatives.

Finally, we find that the white dwarfs in our sample show a strong tendency towards high masses. The high mass dominance implies that the white dwarfs in CVs are not significantly eroded by nova outbursts, and may actually increase over several nova cycles. We find no evidence for He-core white dwarfs within our sample, despite predictions that between 40 and 80 percent of short period CVs should contain He-core white dwarfs.

6 ACKNOWLEDGEMENTS

We would like to thank our referee, Joe Patterson for his useful comments. We also thank Christian Knigge for useful discussions on white dwarf bias and selection effects. CDJS acknowledges the support of an STFC PhD. SPL acknowledges the support of an RCUK Fellowship. CMC and TRM are supported under grant ST/F002599/1 from the Science and Technology Facilities Council (STFC). ULTRACAM and ULTRASPEC are supported by STFC grant ST/G003092/1. This research has made use of NASA's Astrophysics Data System Bibliographic Services. This article is based on observations made with ULTRACAM mounted on the Isaac Newton Group's WHT, and ULTRACAM and ULTRASPEC mounted on the European Southern Observatory's NTT and VLT telescopes.

REFERENCES

Bergeron P., Wesemael F., Beauchamp A., 1995, PASP, 107, 1047
Chabrier G., Gallardo J., Baraffe I., 2007, A&A, 472, L17
Copperwheat C., Marsh T., Dhillon V., Littlefair S., Hickman R., Gänsicke B., Southworth J., 2010, MNRAS, 402, 1824
D'Cruz N., Dorman B., Rood R., O'Connell R., 1996, ApJ, 446, 359
Dhillon V., et al 2007, MNRAS, 378, 825
Epelstain N., Yaron O., Kovetz A., Prialnik D., 2007, MNRAS, 374, 1449
Feline W., 2005, PhD thesis, The University of Sheffield
Feline W., Dhillon V., Marsh T., Stevenson M., Watson C., Brinkworth C., 2004a, MNRAS, 347, 1173
Feline W., Dhillon V., Marsh T., Brinkworth C., 2004b, MNRAS, 355, 1
Ford E., 2006, ApJ, 642, 505
Gänsicke B., Dillon M., Southworth J., Thornstensen J., Rodríguez-Gil P., Aungwerojwit A., Marsh T., et al. 2009, MNRAS, 397, 2170
Gregory P., 2007, MNRAS, 381, 1607
Hamada T., Salpeter E., 1961, ApJ, 134, 683
Hellier C., 2001, Cataclysmic Variable Stars. Praxis Publishing Ltd, Chichester
Horne K., Marsh T., Cheng F., Hubany I., Lanz T., 1994, ApJ, 426, 294
Kepler S., Kleinman S., Nitta A., Koester D., Castanheira B., Giovannini O., Althaus L., 2007, in Napiwotzki R., Burleigh M., eds, 15th European Workshop on White Dwarfs Vol. 372 of ASPCS, The white dwarf mass distribution. pp 35–40
Knigge C., 2006, MNRAS, 373, 484
Kolb U., 1993, A&A, 271, 149
Kolb U., Baraffe I., 1999, MNRAS, 309, 1034
Liebert J., Bergeron P., Holberg J., 2005, ApJS, 156, 47
Littlefair S., Dhillon V., Martn E., 2003, MNRAS, 340, 264
Littlefair S., Dhillon V., Marsh T., Gänsicke B., 2006a, MNRAS, 371, 1435
Littlefair S., Dhillon V., Marsh T., Gänsicke B., Southworth J., Watson C., 2006b, Sci, 314, 1578
Littlefair S., Dhillon V., Marsh T., Gänsicke B., Baraffe I., Watson C., 2007, MNRAS, 381, 827
Littlefair S., Dhillon V., Marsh T., Gänsicke B., Southworth J., Baraffe I., Watson C., Copperwheat C., 2008, MNRAS, 388, 1582
Paczynski B., 1981, Acta Astron., 31, 1
Panei J., Althaus L., Benvenuto O., 2000, A&A, 353, 970
Patterson J., 1998, PASP, 110, 1132
Patterson J., 2009, ArXiv e-prints
Patterson J., Thornstensen J., Knigge C., 2008, PASP, 120, 510
Pickles A., 1998, PASP, 110, 863
Ritter H., 1976, MNRAS, 175, 279
Ritter H., 1985, A&A, 148, 207
Ritter H., Burkert A., 1986, A&A, 158, 161
Roberts G., Gelman A., Gilks W., 1997, Annual of Applied Probability, 7, 110
Robinsons E. L., 1976, ApJ, 203, 485
Sirotkin F. V., Kim W.-T., 2010, ApJ, 721, 1356
Smith D., Dhillon V., 1998, MNRAS, 301, 767
Smith J., et al. 2002, AJ, 123, 2121
Southworth J., Copperwheat C. M., Gänsicke B. T., Pyrzas S., 2010, A&A, 510, A100+
Szkody P., et al. 2004, ApJ, 128, 1882
Szkody P., et al. 2005, ApJ, 129, 2386
Szkody P., et al. 2006, ApJ, 131, 973
Szkody P., et al. 2007, ApJ, 134, 185

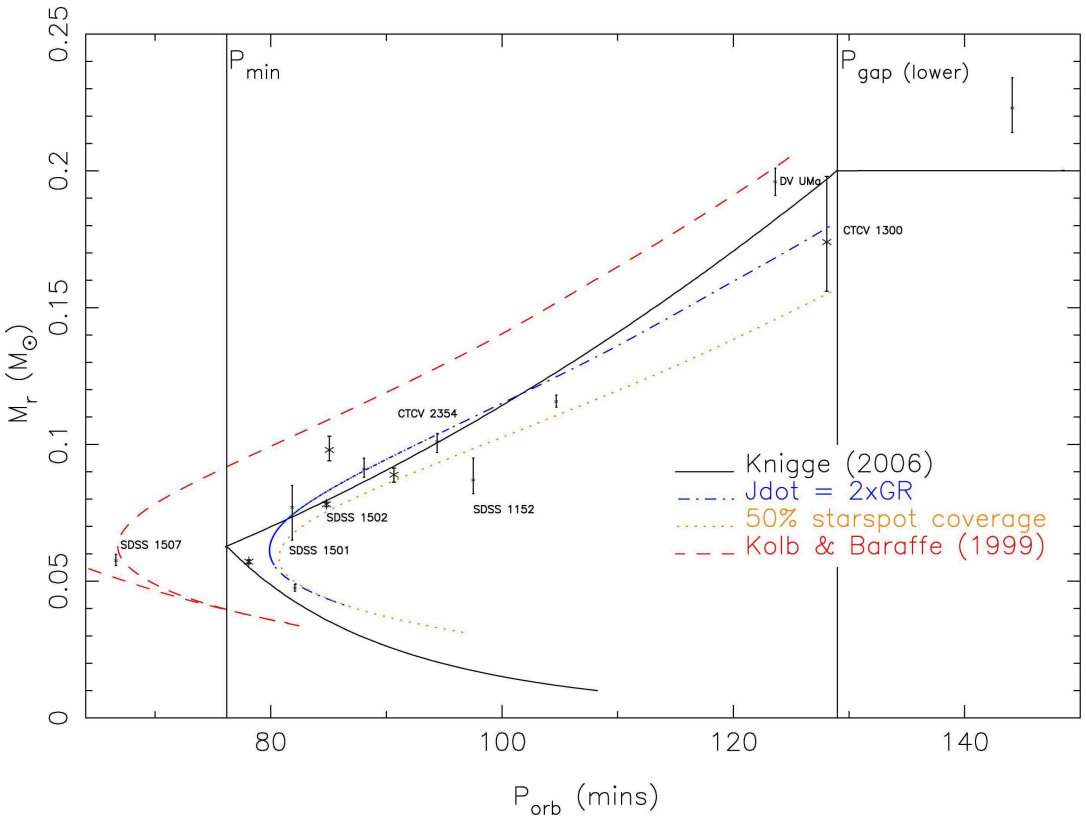

Figure 8. The $M_2 - P_{orb}$ relationship for our dataset. Mass determinations for all systems using ULTRACAM data are included. Our three new systems, in addition to other objects of particular interest are labelled. The evolutionary models of Kolb & Baraffe (1999) calculated with different mass-transfer rates are shown with red (dashed) and blue (dot-dashed) lines. A model with 50 percent star spot coverage on the surface of the donor is shown with an orange (dotted) line. The solid (black) line shows the empirical mass-radius relationship as found by Knigge (2006). The position of the period minimum and period gap, as found by Knigge (2006), are also shown.

Tappert C., Augusteijn T., Maza J., 2004, MNRAS, 354, 321
Townsley D., Gänsicke B., 2009, ApJ, 693, 1007
Tulloch S., Rodríguez-Gil P., Dhillon V., 2009, MNRAS, 397, L82
Warner B., 1973, MNRAS, 162, 189
Warner B., 1976, in IAU Symposium, Vol.73, Structure and Evolution of Close Binary Systems, ed. P. Eggleton, S. Mitton & J.Whelan, 85-+
Warner B., 1995, Cataclysmic Variable Stars. Cambridge University Press, Cambridge
Willems B., Kolb U., Sandquist E., Taam R., Dubus G., 2005, ApJ, 635, 1263
Wood J., Irwin M., Pringle J., 1985, MNRAS, 214, 475
Wood J., Horne K., Berriman G., Wade R., O'Donoghue D., Warner B., 1986, MNRAS, 219, 629
Wood M., 1995, in Koester D., Werner K., eds, LNP Vol. 443, *White Dwarfs.* Springer-Verlag, Berlin. p.41
Yaron O., Prialnik D., Shara M., Kovetz A., 2005, ApJ, 623, 398
Zorotovic, M., Schriber. M.R., Gänsicke., B.T., 2011, *A&A*, *submitted*